

# Effects of Imperfections on Solid-Wave Gyroscope Dynamics

Erdal Yilmaz  
Applied Physics  
Cornell University  
Ithaca, NY 14853  
Email: ey45@cornell.edu

David Bindel  
Department of Computer Science  
Cornell University  
Ithaca, NY 14853  
Email: bindel@cs.cornell.edu

**Abstract**—Solid-wave gyroscopes are symmetric resonators that sense rotation by measuring how Coriolis forces perturb a degenerate mode pair. The idealized dynamics of these devices are described by ODE models of two identical oscillators coupled by a perturbation due to rotation. In miniaturized solid-wave gyroscopes, geometric distortions due to imperfect fabrication also perturb the dynamics, and this limits sensing accuracy. In this work, we describe how geometric imperfections affect the dynamics of solid-wave gyroscopes. We also use selection rules both to find qualitative information about what types of geometry perturbations most affect sensor performance and to accelerate computations.

## I. INTRODUCTION

Hemispherical resonator gyroscopes (HRGs) have become the gyroscope of choice for satellites and other spacecraft [1]. The physics behind the HRG were elucidated by G. H. Bryan in an 1890 experiment that explained the beating sound produced by a ringing wine glass placed on a turntable [2]. When an axisymmetric structure rotates, Coriolis forces break the symmetry between how waves travel clockwise and counter-clockwise: similar to the Doppler effect, elastic waves appear to travel faster or slower depending on the direction in which they travel relative to the rotation. Because of this symmetry breaking, the Coriolis force perturbs degenerate vibration modes, splitting their frequencies in proportion to the rate of rotation. The superposition of beating elastic waves forms a vibration pattern that rotates in the non-inertial reference frame in the direction opposite the frame rotation. Thus, the structure is a *rate-integrating* gyroscope: the rotation of the vibration pattern measures the total rotation of the frame.

The HRG fabrication process yields high-quality, highly axisymmetric resonant structures, but it is expensive. In contrast, MEMS fabrication techniques allow batch production of inexpensive sensors. The community has investigated ring resonators as rate-integrating gyroscopes for over a decade [3], [4], and has recently demonstrated several methods to fabricate hemispherical shells [5], [6], [7]. However, microfabrication introduces geometric imperfections in many processing steps. These imperfections decrease the sensing accuracy considerably compared to macro gyroscopes. Understanding these imperfections is important for predicting sensor quality and formulating rules of thumb for device design.

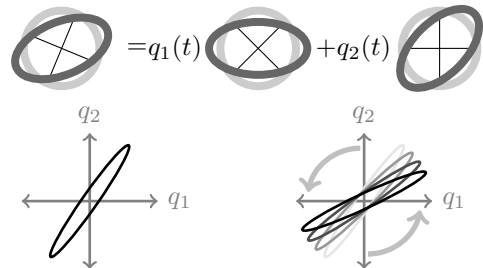


Fig. 1. A solid-wave gyro oscillates in a space defined by two degenerate modes (shown at top for a ring gyro in an  $m = 2$  mode). In a stationary frame,  $\mathbf{q}(t)$  oscillates in an elliptical trajectory (left); rotation of the frame at rate  $\Omega$  causes this ellipse to rotate at rate  $-\beta\Omega$  (right).

## II. BACKGROUND

In a solid-wave gyroscope, Coriolis forces couple oscillations in a degenerate pair of vibration modes of an axisymmetric structure. Let  $\hat{\mathbf{u}}^1$  and  $\hat{\mathbf{u}}^2$  be a pair of degenerate modes with  $m \geq 1$  in which the radial displacements vary like  $\cos(m\theta)$  and  $\sin(m\theta)$ , respectively. The displacement field for a free vibration is then

$$\mathbf{u}(r, z, \theta, t) \approx \hat{\mathbf{u}}^1(r, z, \theta)q_1(t) + \hat{\mathbf{u}}^2(r, z, \theta)q_2(t), \quad (1)$$

where  $q_1$  and  $q_2$  are determined by the lumped model equation

$$\ddot{\mathbf{q}} + 2\beta\Omega\mathbf{J}\dot{\mathbf{q}} + \omega_0^2\mathbf{q} = 0, \quad \mathbf{J} \equiv \begin{bmatrix} 0 & -1 \\ 1 & 0 \end{bmatrix}, \quad (2)$$

where  $\Omega \ll \omega_0$  is the rotational velocity about the sense axis. When  $\Omega = 0$ ,  $q_1$  and  $q_2$  are decoupled, so solutions to (2) follow elliptical trajectories with frequency  $\omega_0$ . For constant, nonzero rotations, the coupled system vibrates at two characteristic frequencies  $\omega \approx \omega_0 \pm \beta\Omega$ . Interference of these vibrations gives a slower beat frequency that has a simple geometric interpretation (Figure 1): if  $\mathbf{q}^0(t)$  is an elliptical phase space trajectory at  $\Omega = 0$ , then beating causes this ellipse to effectively rotate in the configuration space:

$$\begin{bmatrix} q_1(t) \\ q_2(t) \end{bmatrix} \approx \begin{bmatrix} \cos(-\beta\Omega t) & -\sin(-\beta\Omega t) \\ \sin(-\beta\Omega t) & \cos(-\beta\Omega t) \end{bmatrix} \begin{bmatrix} q_1^0(t) \\ q_2^0(t) \end{bmatrix}.$$

The same basic picture holds when the rotation rate varies slowly ( $\dot{\Omega} \ll \omega_0^2$ ), so that the total rotation of the ellipse is proportional to the total rotation of the frame. A rotation of

$\pi/2$  in configuration space moves from one mode to the other; that is, it corresponds to a rotation of the vibration pattern by  $\pi/(2m)$ . Therefore, the angular gain for the gyroscope is

$$\text{Bryan's factor} \equiv \frac{\text{Rotation of the vibration pattern}}{\text{Rotation of the vibrating body}} = \frac{\beta}{m}.$$

### III. DISTRIBUTED-PARAMETER MODELING

The weak form of linear elasticity is

$$\forall \mathbf{w} \in \mathcal{V}, \quad b(\mathbf{w}, \mathbf{a}) + a(\mathbf{w}, \mathbf{u}) = F(\mathbf{w}), \quad (3)$$

$$b(\mathbf{w}, \mathbf{a}) = \int_{\mathcal{B}} \rho \mathbf{w} \cdot \mathbf{a} \, d\mathcal{B},$$

$$a(\mathbf{w}, \mathbf{u}) = \int_{\mathcal{B}} \boldsymbol{\varepsilon}(\mathbf{w}) : \mathbf{C} : \boldsymbol{\varepsilon}(\mathbf{u}) \, d\mathcal{B}, \quad F(\mathbf{w}) = \int_{\mathcal{B}} \mathbf{w} \cdot \mathbf{f} \, d\mathcal{B}.$$

where  $\mathbf{u}$  and  $\mathbf{a}$  are the displacement and acceleration fields,  $\rho$  and  $\mathbf{C}$  are the mass density and the elasticity tensor,  $\mathcal{B}$  is the body, and  $\mathcal{V}$  is the space of admissible displacements. In a rotating frame with rotation vector  $\boldsymbol{\Omega}$ , we write

$$\mathbf{a} = \ddot{\mathbf{u}} + 2\boldsymbol{\Omega} \times \dot{\mathbf{u}} + \boldsymbol{\Omega} \times (\boldsymbol{\Omega} \times \mathbf{x}) + \dot{\boldsymbol{\Omega}} \times \mathbf{x} \quad (4)$$

where  $\mathbf{r}$  is the undeformed position vector and  $\mathbf{x} = \mathbf{r} + \mathbf{u}$ . The last three terms in (4) give rise to *fictitious forces*: the Coriolis force, the centrifugal force, and the Euler force. Substituting (4) into (3) yields the weak form for linear elasticity in a rotating frame, including fictitious forces:

$$\forall \mathbf{w} \in \mathcal{V}, \quad b(\mathbf{w}, \ddot{\mathbf{u}}) + 2b(\mathbf{w}, \boldsymbol{\Omega} \times \dot{\mathbf{u}}) + \tilde{a}(\mathbf{w}, \mathbf{u}) = \tilde{F}(\mathbf{w}), \quad (5)$$

$$\tilde{a}(\mathbf{w}, \mathbf{u}) = a(\mathbf{w}, \mathbf{u}) + b(\mathbf{w}, \boldsymbol{\Omega} \times (\boldsymbol{\Omega} \times \mathbf{u}) + \dot{\boldsymbol{\Omega}} \times \mathbf{u}), \quad (6)$$

$$\tilde{F}(\mathbf{w}) = F(\mathbf{w}) - b(\mathbf{w}, \boldsymbol{\Omega} \times (\boldsymbol{\Omega} \times \mathbf{r}) + \dot{\boldsymbol{\Omega}} \times \mathbf{r}). \quad (7)$$

We assume small rotational velocities and accelerations, i.e.  $\|\boldsymbol{\Omega}\| \ll \omega_0$  and  $\|\dot{\boldsymbol{\Omega}}\| \ll \omega_0^2$ , and so  $\tilde{a} \approx a$  and  $\tilde{F} \approx F$ .

We use cylindrical polar coordinates to parameterize the geometry and the vector fields. That is,  $\mathbf{u}$  represents

$$\mathbf{u}(r, \theta, z) = \begin{bmatrix} u_r \\ u_\theta \\ u_z \end{bmatrix} = \begin{bmatrix} \cos(\theta)u_x - \sin(\theta)u_y \\ \sin(\theta)u_x + \cos(\theta)u_y \\ u_z \end{bmatrix},$$

and similarly with  $\mathbf{w}$ . We also write  $\boldsymbol{\Omega}$  in polar form as

$$\boldsymbol{\Omega} = \Omega_z \mathbf{e}_z + \boldsymbol{\Omega}_{r\theta} = \begin{bmatrix} 0 \\ 0 \\ \Omega_z \end{bmatrix} + \begin{bmatrix} \cos(\theta)\Omega_x - \sin(\theta)\Omega_y \\ \sin(\theta)\Omega_x + \cos(\theta)\Omega_y \\ 0 \end{bmatrix}.$$

We expand  $\mathbf{u} = \mathbf{u}^c + \mathbf{u}^s$  in the Fourier series

$$\mathbf{u}^c = \sum_{m=0}^{\infty} \boldsymbol{\Phi}_m^c(\theta) \mathbf{u}_m^c(r, z), \quad \mathbf{u}^s = \sum_{m=0}^{\infty} \boldsymbol{\Phi}_m^s(\theta) \mathbf{u}_m^s(r, z)$$

where  $\boldsymbol{\Phi}^c(\theta)$  and  $\boldsymbol{\Phi}^s(\theta)$  are the diagonal matrices

$$\boldsymbol{\Phi}_m^c(\theta) = \text{diag}(\cos(m\theta), \sin(m\theta), \cos(m\theta)) \quad (8)$$

$$\boldsymbol{\Phi}_m^s(\theta) = \text{diag}(-\sin(m\theta), \cos(m\theta), -\sin(m\theta)). \quad (9)$$

We say  $\mathbf{u}$  has a single azimuthal number  $m$  if  $\mathbf{u}_m^c$  and  $\mathbf{u}_m^s$  are the only nonzero terms in the Fourier expansion of  $\mathbf{u}$ .

Based on these expansions, we define reduced bilinear forms

$$a_{mn}^{xy}(\mathbf{w}_m^x, \mathbf{u}_n^y) = a(\boldsymbol{\Phi}_m^x \mathbf{w}_m^x, \boldsymbol{\Phi}_n^y \mathbf{u}_n^y)$$

for  $x, y \in \{c, s\}$ . We similarly define reduced forms for  $b$ . Symmetry of  $a$  and  $b$  implies  $a_{mn}^{cs} = a_{nm}^{sc}$  and  $b_{mn}^{cs} = b_{nm}^{sc}$ .

If  $\rho$  and  $\mathbf{C}$  are independent of  $\theta$ , then  $a$  and  $b$  are diagonal in the Fourier basis:  $a_{mn}^{cc}$  and  $a_{mn}^{ss}$  are nonzero only when  $m = n$ , and  $a_{mn}^{cs} = a_{mn}^{sc} = 0$  for all  $m$  and  $n$ ; and similarly with  $b$ . Thus, when there is no rotation, equation (3) decouples into a pair of 2D problems for each wave number  $m$ . We also decouple the problem of finding modes in an inertial frame; this gives

$$\forall \mathbf{w}_m \in \mathcal{V}_m, \quad -\omega^2 b_{mm}^{cc}(\mathbf{w}_m, \hat{\mathbf{u}}_m) + a_{mm}^{cc}(\mathbf{w}_m, \hat{\mathbf{u}}_m) = 0, \quad (10)$$

and a similar problem involving  $b_{mm}^{ss}$  and  $a_{mm}^{ss}$ . For  $m > 0$ , these two problems yield modes with the same shape, differing only by a rotation of  $\pi/(2m)$ ; that is, for  $m > 0$ , modes come in degenerate pairs with the same frequency.

The Coriolis term does *not* generally diagonalize in the Fourier basis. We treat the Coriolis effect in an axisymmetric system in two pieces. By bilinearity of  $b$ ,

$$b(\mathbf{w}, \boldsymbol{\Omega} \times \mathbf{u}) = \Omega_z b(\mathbf{w}, \mathbf{e}_z \times \mathbf{u}) + b(\mathbf{w}, \boldsymbol{\Omega}_{r\theta} \times \mathbf{u}).$$

If  $\mathbf{w}$  has a single azimuthal number  $m$  and  $\mathbf{u}$  has a single azimuthal number  $n$ , then  $b(\mathbf{w}, \mathbf{e}_z \times \mathbf{u})$  may only be nonzero for  $m = n$ . On the other hand,  $\boldsymbol{\Omega}_{r\theta}$  has azimuthal number 1; thus,  $\boldsymbol{\Omega}_{r\theta} \times \mathbf{u}$  will generally have azimuthal numbers  $n \pm 1$ , and so  $b(\mathbf{w}, \boldsymbol{\Omega}_{r\theta} \times \mathbf{u})$  may be nonzero only for  $m = n \pm 1$ .

The Fourier decomposition of  $\mathbf{u}$  is also the basis for a fast ‘‘2.5d’’ finite element method. We write our approximate displacement  $\mathbf{u}^h$  as

$$\mathbf{u}^h(r, z, \theta) = \sum_{m=0}^M \sum_{l=0}^L N_l(r, z) [\boldsymbol{\Phi}_m^c(\theta) \mathbf{u}_{ml}^c + \boldsymbol{\Phi}_m^s(\theta) \mathbf{u}_{ml}^s],$$

where  $N_l(r, z)$  are ordinary finite element shape functions on the 2D cross section. Substituting this expression into (5) gives us the finite element system

$$\mathbf{M} \ddot{\mathbf{u}}^h + \mathbf{C} \dot{\mathbf{u}}^h + \mathbf{K} \mathbf{u}^h = \mathbf{f}^h,$$

where  $\mathbf{M}$  and  $\mathbf{K}$  are the usual symmetric mass and stiffness matrices and  $\mathbf{C}$  is a skew-symmetric matrix that arises from the Coriolis term in (5). We will typically order the unknowns first by  $m$ , then by whether the shape function is symmetric or antisymmetric, and then by  $l$ . When the material properties are also rotationally invariant,  $\mathbf{M}$  and  $\mathbf{K}$  inherit the block diagonal structure of  $a$  and  $b$ , and  $\mathbf{C}$  is block tridiagonal.

For  $m > 0$ , let  $\hat{\mathbf{u}}^1 = \boldsymbol{\Phi}_m^c \hat{\mathbf{u}}_m$  and  $\hat{\mathbf{u}}^2 = \boldsymbol{\Phi}_m^s \hat{\mathbf{u}}_m$  be a degenerate mode pair in the inertial frame, scaled so  $b(\hat{\mathbf{u}}^j, \hat{\mathbf{u}}^k) = \delta_{jk}$ . We derive the lumped model (2) from the assumption (1) and the Galerkin condition

$$\forall j \in \{1, 2\}, \quad b(\hat{\mathbf{u}}^j, \ddot{\mathbf{u}}) + 2b(\hat{\mathbf{u}}^j, \boldsymbol{\Omega} \times \dot{\mathbf{u}}) + a(\hat{\mathbf{u}}^j, \mathbf{u}) = 0. \quad (11)$$

Then  $\Omega_z$  is the sensed rotation and

$$\beta = b(\hat{\mathbf{u}}^2, \mathbf{e}_z \times \hat{\mathbf{u}}^1) = 2\pi \int \hat{u}_{mr} \hat{u}_{mz} \, dr \, dz$$

depends only on the geometry and mode. For  $\boldsymbol{\Omega}_{r\theta} \neq 0$ , the lumped model neglects coupling terms from the Coriolis effect; but these terms are  $O(\|\boldsymbol{\Omega}\|^2/\omega_0^2)$ , comparable to the neglected centrifugal effect.

#### IV. IMPERFECTIONS

While (2) is a good model of an ideal gyroscope, real devices are affected by damping and asymmetries. A more realistic lumped model treats these effects as perturbations:

$$(\mathbf{I} + \delta\tilde{\mathbf{M}})\ddot{q} + (2\beta\Omega\mathbf{J} + \delta\tilde{\mathbf{C}})\dot{q} + (\mathbf{I} + \delta\tilde{\mathbf{K}})\omega_0^2 q = 0. \quad (12)$$

Several researchers have investigated how such perturbations affect the dynamics of the lumped model [8], [9], [10], but there has been relatively little work on computation of the perturbation matrices. Our focus is the analysis and computation of perturbations due to geometric distortions.

We write the distorted geometry  $\mathcal{B}$  as the image of an axisymmetric reference geometry  $\mathcal{B}_0$  under a mapping:

$$\mathbf{R} \in \mathcal{B}_0 \mapsto \mathbf{r} = \mathbf{R} + \epsilon\psi(\mathbf{R}) \in \mathcal{B}, \quad (13)$$

where  $\mathbf{R} = (r_0, z_0, \theta_0)$  and  $\mathbf{r} = (r, z, \theta)$ . We give an example in Figure 3. In terms of the reference geometry, we have

$$b(\mathbf{w}, \mathbf{a}) = \int_{\mathcal{B}_0} \rho \mathbf{w} \cdot \mathbf{a} J d\mathcal{B}_0,$$

$$a(\mathbf{w}, \mathbf{u}) = \int_{\mathcal{B}_0} \boldsymbol{\varepsilon}(\mathbf{w}) : \mathbf{C} : \boldsymbol{\varepsilon}(\mathbf{u}) J d\mathcal{B}_0,$$

where  $J = \det(\mathbf{I} + \epsilon\mathbf{F})$  with  $\mathbf{F} = \partial\psi/\partial\mathbf{R}$ . As before, we write Fourier expansions for  $\mathbf{u}$  and  $\mathbf{w}$  in the reference coordinate system. Unlike in the axisymmetric case,  $a$  and  $b$  are not generally diagonal in the Fourier basis. However, we gain insight from determining what part of  $a$  or  $b$  must be small or zero based on the structure of the perturbation.

Abstractly, both  $a$  and  $b$  are defined by integrals in which the integrand depends on  $\epsilon$  via  $\mathbf{r}$  and  $\nabla_{\mathbf{R}}\mathbf{r}$ :

$$\int_{\mathcal{B}_0} f(\mathbf{r}(\epsilon), \nabla_{\mathbf{R}}\mathbf{r}(\epsilon)) d\Omega.$$

Expanding the integrand with respect to  $\epsilon$ , we have

$$f = f|_{\epsilon=0} + \epsilon \left( \left. \frac{\partial f}{\partial \mathbf{r}} \right|_{\epsilon=0} \psi + \left. \frac{\partial f}{\partial \nabla_{\mathbf{R}}\mathbf{r}} \right|_{\epsilon=0} \mathbf{F} \right) + O(\epsilon^2).$$

If  $\psi$ ,  $\mathbf{w}$ , and  $\mathbf{u}$  are at azimuthal numbers  $p$ ,  $m$ , and  $n$ , then the constant (in  $\epsilon$ ) term in the expansion involves products with terms at azimuthal number  $m$  and  $n$ , which integrate to zero except when  $m = n$ ; and the term at order  $\epsilon$  involves products with terms at azimuthal number  $m$ ,  $n$ , and  $p$ , which integrate to zero except when  $m \pm n \pm p = 0$ .

More generally, suppose that the perturbed geometry has  $p$ -fold rotational symmetry. In this case, *selection rules* tell us that if  $\mathbf{w}$  and  $\mathbf{u}$  have azimuthal wave numbers  $m$  and  $n$ , then  $a(\mathbf{w}, \mathbf{u}) = 0$  unless  $m \pm n \pm kp = 0$  for some integer  $k$ . We also know that modes at azimuthal wave number  $m$  remain degenerate under the perturbation unless  $p$  evenly divides  $2m$ :  $\cos(m(\theta + 2\pi/p))$  and  $\cos(m\theta)$  are linearly independent functions on  $[0, 2\pi)$  if  $2\pi m/p$  is not a multiple of  $\pi$ , so if  $\hat{\mathbf{u}}$  is a mode with  $\hat{\mathbf{u}}_m^c$  or  $\hat{\mathbf{u}}_m^s$  nonzero, then  $\hat{\mathbf{u}}(r, z, \theta)$  and  $\hat{\mathbf{u}}(r, z, \theta + 2\pi/p)$  are linearly independent.

We use selection rules *computationally* as part of a fast finite element scheme for analyzing nearly-axisymmetric structures.

For a perturbation with  $p$ -fold rotational symmetry, the matrices  $\mathbf{M}$ ,  $\mathbf{C}$ , and  $\mathbf{K}$  have zero blocks according to the selection rules. Thus, to compute the distorted modes with azimuthal number  $m$ , we use a reduced system in which we only keep  $\mathbf{K}_{\mu\nu}$  where  $|\mu - \nu| = m \pmod{p}$ , and similarly with  $\mathbf{M}$ .

Reasoning purely from symmetry, we can also describe *qualitatively* how a perturbation at mode  $p$  affects a solid-wave gyroscope operating at azimuthal number  $m$ :

- 1) If  $p = 2m$ , the modal mass and stiffness are perturbed by  $O(\epsilon)$ , and frequencies split by  $O(\epsilon)$ .
- 2) If  $p \neq 2m$  evenly divides  $2m$ , the modal mass and stiffness are perturbed by at most  $O(\epsilon^2)$ .
- 3) Otherwise, the modal mass and stiffness are perturbed by at most  $O(\epsilon^2)$ . Frequencies change, but do *not* split. The lumped model (11) remains valid, though the frequency of the operating modes may change by  $O(\epsilon^2)$ .
- 4) If  $p = 1$  or  $p = 2m \pm 1$ , there may be an  $O(\epsilon)$  cross-axis coupling effect: that is, in addition to sensing the rotation about  $z$ , the gyroscope will also sense rotation in  $x$  and  $y$ . If  $lp = 2m \pm 1$ , the coupling occurs at  $O(\epsilon^l)$ .

Some fabrication errors that occur in MEMS can be characterized by a few dominant terms in the Fourier expansion of the geometry. At  $p = 0$  are isotropic under- and over-etching effects, which do not disturb symmetry. At  $p = 1$ , there are effects such as mask misalignment, thickness variations due to proximity to a gas jet, and variations in sidewall slant during a reactive ion etch. At  $p = 2$  are any effects that might stretch the geometry along a single axis, and at  $p = 4$  are ‘‘squaring off’’ effects due to anisotropic etching in a 111 wafer.

The  $m = 2$  modes are affected at first order by  $p = 0$  and  $p = 4$  perturbations, and may also suffer an  $O(\epsilon^2)$  frequency splitting from perturbations at  $p = 1$  or  $p = 2$ . In contrast, the  $m = 3$  modes are affected at first order by  $p = 0$  and  $p = 6$  perturbations, and may suffer an  $O(\epsilon^2)$  frequency split from perturbations at  $p = 3$ . This means that, though the  $m = 3$  shape may be distorted, it will remain degenerate under the fabrication effects we consider, except those at  $p = 1$ .

#### V. ANALYSIS OF A RING RESONATOR

In prior work, researchers have studied geometric imperfections of the ring resonator and quantified frequency splittings [11], [12]. The computations in these papers are based on beam and shell models, and are restricted to in-plane resonators with simple geometry. Our approach, based on a structured three-dimensional finite element analysis, enables the study of more complex geometries in the same framework. Nonetheless, to validate our observations, the ring resonator provides an excellent example.

Our computations reproduce the results of earlier work, and illustrate the qualitative analysis from Section IV. In Figure 2, we see a first order splitting of modes at azimuthal number  $m$  by perturbations with azimuthal number  $p = 2m$ , and a second order splitting for the case  $p = m$ . For most of the values, the frequencies do not split, but decrease together. Figure 3 shows the  $m = 2$  mode shapes for an undeformed ring and for a ring deformed at  $p = 3$  and  $p = 4$ . While the modes in the  $p = 4$

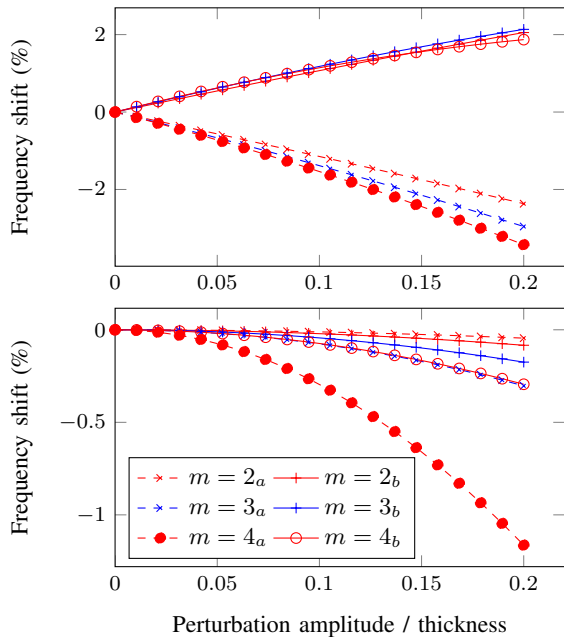


Fig. 2. First-order (top) and second-order (bottom) splittings of degenerate mode frequencies with azimuthal number  $m$  under the perturbation shapes  $\psi(r, \theta) = (\cos(2m\theta), 0)$  and  $\psi(r, \theta) = (\cos(m\theta), 0)$ .

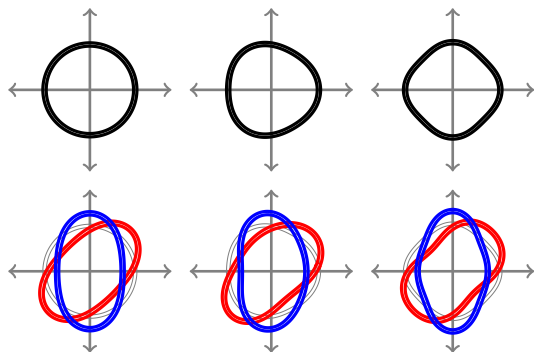


Fig. 3. Top: ideal ring geometry  $B_0$  (left) and distorted geometries under  $\psi(r, \theta) = (\cos(p\theta), 0)$  for  $p = 3$  (center) and  $p = 4$  (right). Bottom:  $m = 2$  mode shapes for the ideal and distorted geometries.

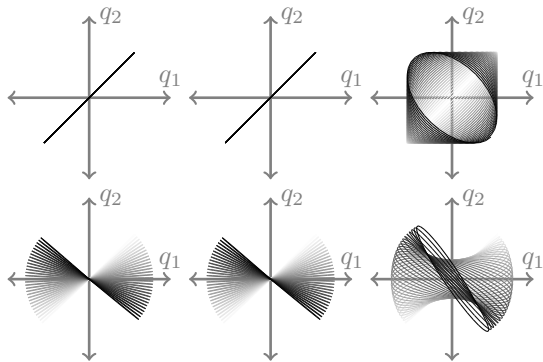


Fig. 4. Top: configuration space dynamics for the ring gyroscopes in Figure 3 in a non-rotating frame over thirty periods. Bottom: configuration space dynamics in a frame rotating at  $\Omega = \omega/200$  over thirty periods.

case have different frequencies and shapes, the modes in the  $p = 3$  case remain degenerate, and have the same basic shape.

Figure 4 shows the configuration-space trajectories for the deformed ring gyroscopes shown in Figure 3. The  $p = 3$  perturbation only affects the frequency of oscillation and Bryan's factor, and those by only a small amount. The configuration space dynamics are visually indistinguishable from the unperturbed case, despite the relatively large deformation. In contrast, the  $p = 4$  perturbation significantly affects the dynamics even in a stationary frame. The picture in a rotating frame is also significantly distorted.

## VI. CONCLUSION

Miniaturized solid-wave gyroscopes are a promising technology, but the precision of such devices is limited by geometric imperfections due to fabrication issues. To understand this challenge, we want to understand how different imperfections affect dynamics in the modes used for sensing. By writing the mode shapes and imperfection shape as Fourier series, we can apply selection rules to reason about which types of imperfections most strongly perturb the dynamics used for sensing. Our approach yields rules for reasoning qualitatively about different types of imperfections, and also provides the basis for a fast finite element method for computing the effect of specific imperfections.

## REFERENCES

- [1] D. M. Rozelle. The hemispherical resonator gyro: From wineglass to the planets. Northrop Grumman Co. [Online]. Available: [www.northropgrumman.com/Capabilities/HRG/Documents/hrg.pdf](http://www.northropgrumman.com/Capabilities/HRG/Documents/hrg.pdf)
- [2] G. H. Bryan, "On the beats in the vibrations of a revolving cylinder or bell," *Proc. Cambridge Philos. Soc.*, vol. 7, pp. 101–111, 1890.
- [3] F. Ayazi and K. Najafi, "A HARPSS polysilicon vibrating ring gyroscope," *J. MEMS*, vol. 10, no. 2, pp. 169–179, 2001.
- [4] G. He and K. Najafi, "A single-crystal silicon vibrating ring gyroscope," in *Proc. IEEE MEMS*, 2002, pp. 718–721.
- [5] K. Visvanathan, T. Li, and Y. B. Gianchandani, "3D-soule: A fabrication process for large scale integration and micromachining of spherical structures," in *Proc. IEEE MEMS*, 2011, pp. 45–48.
- [6] L. D. Sorenson, X. Gao, and F. Ayazi, "3-D micromachined hemispherical shell resonators with integrated capacitive transducers," in *Proc. IEEE MEMS*, 2012, pp. 168–171.
- [7] J. Cho, J. Yan, J. A. Gregory, H. Eberhart, R. L. Peterson, and K. Najafi, "High-Q fused silica birdbath and hemispherical 3-D resonators made by blow torch molding," in *Proc. IEEE MEMS*, 2013, pp. 177–180.
- [8] B. Friedland and M. Hutton, "Theory and error analysis of vibrating-member gyroscope," *IEEE Trans. Automat. Control*, vol. 23, no. 4, pp. 545–556, 1978.
- [9] A. M. Shkel, R. T. Howe, and R. Horowitz, "Modeling and simulation of micromachined gyroscopes in the presence of imperfections," in *Proc. Modeling and Simulation of Microsystems*, 1999.
- [10] D. M. Klimov and V. P. Zhuravlev, *Group-theoretic methods in mechanics and applied mathematics*. New York: Taylor & Francis, 2002.
- [11] R. S. Hwang, C. H. J. Fox, and S. McWilliam, "The in-plane vibration of thin rings with in-plane profile variations part I: General background and theoretical formulation," *J. Sound Vibration*, vol. 220, no. 3, pp. 497–516, 1999.
- [12] C. H. J. Fox, R. S. Hwang, and S. McWilliam, "The in-plane vibration of thin rings with in-plane profile variations part II: Application to nominally circular rings," *Journal of Sound and Vibration*, vol. 220, no. 3, pp. 517–539, 1999.